

See discussions, stats, and author profiles for this publication at: <https://www.researchgate.net/publication/261097567>

A Series of Four-Connected Entangled Metal-Organic Frameworks Assembled from Pamoic Acid and Pyridine-Containing Ligands: Interpenetrating, Self-Penetrating, and Supramolecular Iso...

ARTICLE in CRYSTAL GROWTH & DESIGN · JANUARY 2012

Impact Factor: 4.89 · DOI: 10.1021/cg2008057

CITATIONS

41

READS

12

9 AUTHORS, INCLUDING:



Ruirui Yun

Anhui Normal University

29 PUBLICATIONS 286 CITATIONS

[SEE PROFILE](#)



Qingfu Zhang

Liaocheng Universtiy

29 PUBLICATIONS 393 CITATIONS

[SEE PROFILE](#)



Jing Lu

163 PUBLICATIONS 1,386 CITATIONS

[SEE PROFILE](#)



Junfeng Bai

Nanjing University

73 PUBLICATIONS 3,027 CITATIONS

[SEE PROFILE](#)

A Series of Four-Connected Entangled Metal–Organic Frameworks Assembled from Pamoic Acid and Pyridine-Containing Ligands: Interpenetrating, Self-Penetrating, and Supramolecular Isomerism

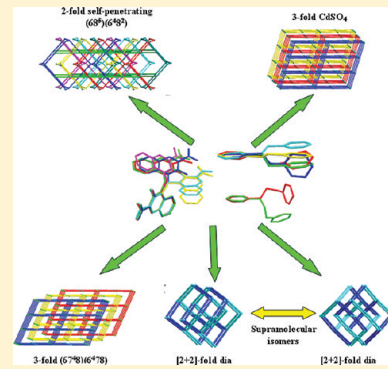
Suna Wang,^{†,‡} Ruirui Yun,[‡] Yanqiang Peng,[†] Qingfu Zhang,[†] Jing Lu,[†] Jianmin Dou,^{*,†} Junfeng Bai,^{*,‡} Dacheng Li,[†] and Daqi Wang[†]

[†]Shandong Provincial Key Laboratory of Chemical Energy Storage and Novel Cell Technology, School of Chemistry and Chemical Engineering, LiaoCheng University, LiaoCheng, 252059, P. R. China

[‡]State Key Laboratory of Coordination Chemistry, School of Chemistry and Chemical Engineering, Nanjing National Laboratory of Microstructures, Nanjing University, Nanjing, P. R. China

Supporting Information

ABSTRACT: Five novel compounds, $\{[\text{Ni}(\text{PA})(\text{bpe})(\text{H}_2\text{O})_2] \cdot \text{DMF}\}_n$ (**1**), $\{[\text{Zn}(\text{PA})(\text{bpe})] \cdot \text{DMF}\}_n$ (**2**), $\{[\text{Zn}(\text{PA})(\text{bpe})] \cdot 2\text{DMF} \cdot \text{CH}_3\text{OH}\}_n$ (**3**), $\{[\text{Cd}_2(\text{PA})_2(\text{bpe})_2(\text{H}_2\text{O})] \cdot 3\text{SH}_2\text{O}\}_n$ (**4**), $\{[\text{Ni}_2(\text{PA})_2(\text{bpp})_2(\text{H}_2\text{O})_3] \cdot 2\text{DMF}\}_n$ (**5**), based on pamoic acid (H_2PA) ($\text{bpe} = 1,2\text{-bi}(4\text{-pyridyl})\text{ethane}$, $\text{bpp} = 1,3\text{-bi}(4\text{-pyridyl})\text{propane}$) have been synthesized. In such a system, both the PA^{2-} anion ligand and dipyridyl ligands act as bipodal linkers, connecting the metal centers in square or tetrahedral geometries into 4-connected topologies with different entangled modes: 3-fold interpenetrating CdSO_4 net ($6^5.8$) (**1**), roto-translational $[2+2]$ interpenetrating diamond pseudosupramolecular isomers (**2** and **3**), 3-fold interpenetrating ($6.7^4.8)(6^4.7.8$) (**4**) and ($6.8^5)(6^4.8^2$) net with both 2-fold interpenetrating and self-penetrating characters (**5**), respectively. The formation of unique penetrating frameworks was investigated in detail. Gas adsorption and photoluminescent properties of the compounds have also been explored.



■ INTRODUCTION

The assembly of metal–organic frameworks (MOFs) is attracting more attention in the field of supramolecular chemistry and crystal engineering in recent years.^{1–3} Entanglement motifs are of great interest, which have been reviewed recently by Batten, Robson, and Ciani and co-workers.^{4–7} Such systems not only exhibit a variety of architectures but also show intriguing properties for potential applications, such as gas adsorption, molecular electronic devices, and so on. The exploitation of these structures can be helpful for both the design and analysis of crystal structures and understanding the relationships between the structure and function of these coordination polymers. Considering the complicated factors that could have influences on the resulting networks, however, the prediction and design of entangled networks are still a great challenge.

Among such systems interpenetrating and self-interpenetrating networks are most widely investigated. The former can be described as a number of individual nets participating in interpenetration with each other. The latter, however, are single nets having the peculiarity that the smallest topological rings are catenated by other rings belonging to the same net. In most of these entangled structures, long flexible ligands were always employed, especially those long and V-shaped polycarboxylate tectons together with flexible exo-bidentate N-heterocycle ligands, such as 4,4'-sulfonyldibenzonic acid (H_2sdba), 4,4'-dicarboxy-2,2'-bipyridine acid (H_2dcbp), 2,2'-dithiobisbenzoic acid (H_2dtba),

4,4'-oxybis(benzoate) (H_2oba), 4-(4-carboxyphenoxy)phthalic acid (H_2cpp), 1,3-bis(4-pyridyl)propane (bpp), 1,4-bis(1-imidazol-yl)-benzene (bib), 1,2-bis(1,2,4-triazol-4-yl)-butane (bbi), and so on.^{8,9} The entangled mode is strongly related to the length and flexibility of the spacer ligands. Generally, the larger the voids and the lower the coordination number of metal centers, the more likely penetration occurs and the more individual nets penetrate each other.

Previously, we have reported a few fascinating entangled structures using flexible dicarboxylate or tricarboxylate ligands, including 4,4'-(carbonylimino)dibenzonic acid, $N,N',N''\text{-}1,3,5\text{-triazine-2,4,6-triyltrisglycine}$ and 1,3,5-tris(carboxymethoxy)-benzene.¹⁰ Along with this work in such fields, we selected pamoic acid (H_2PA , 4,4'-methylenebis(3-hydroxy-2-naphthalenecarboxylic acid)) as a building unit. Coexistence of naphthalene rings and the central sp^3 carbon atom makes this long V-shaped aromatic dicarboxylate ligand possess both rigid and flexible characters.¹¹ Combination of flexible exo-bidentate N-containing ligands with this ligand may lead to exciting structures. Herein, we reported five novel compounds: $\{[\text{Ni}(\text{PA})(\text{bpe})(\text{H}_2\text{O})_2] \cdot \text{DMF}\}_n$ (**1**), $\{[\text{Zn}(\text{PA})(\text{bpe})] \cdot \text{DMF}\}_n$ (**2**), $\{[\text{Zn}(\text{PA})(\text{bpe})] \cdot 2\text{DMF} \cdot \text{CH}_3\text{OH}\}_n$ (**3**), $\{[\text{Cd}_2(\text{PA})_2(\text{bpe})(\text{H}_2\text{O})] \cdot 3\text{SH}_2\text{O}\}_n$ (**4**), $\{[\text{Ni}_2(\text{PA})_2(\text{bpp})_2(\text{H}_2\text{O})_3] \cdot 2\text{DMF}\}_n$ (**5**).

Received: June 25, 2011

Revised: October 23, 2011

Published: November 07, 2011

(**5**), (*bpe* = 1,2-bi(4-pyridyl)ethane, *bpp* = 1,3-bi(4-pyridyl)propane). PA²⁻ and *bpe/bpp* connect the metal centers in square-planar or tetrahedral geometries into 4-connected topologies with interesting interpenetrating or self-penetrating modes: 3-fold interpenetrating CdSO₄ (6^{5.8}) (**1**), pseudosupramolecular isomeric roto-translational [2 + 2] interpenetrating diamondoid network (**2** and **3**), 3-fold interpenetrating (6.7^{4.8})(6^{4.7.8}) net (**4**), and 2-fold interpenetrating self-penetrating (6.8⁵)(6^{4.8²}) net (**5**), respectively. The importance of the conformations of the PA²⁻ ligand and other flexible coligand as well as metal ions in the formation of unique frameworks was unraveled. Gas adsorption and photoluminescent properties of these compounds have also been explored.

■ EXPERIMENTAL SECTION

General Methods. Pamoic acid was purchased from Alfa-aesar. 1,2-Bi(4-pyridyl)ethane (*bpe*) and 1,3-bi(4-pyridyl)propane (*bpp*) were purchased from Sigma-Aldrich. Other reagents were commercially available and used as purchased without further purification. The elemental analysis was carried out with a Perkin-Elmer 240C elemental analyzer. The FT-IR spectra were recorded from KBr pellets in the range of 4000–400 cm⁻¹ on a VECTRA 22 spectrometer. Powder X-ray diffraction (PXRD) data were collected over the 2θ range 5–50° on a Philips X'pert diffractometer using Cu Kα radiation ($\lambda = 1.5418 \text{ \AA}$) at room temperature. Thermal analyses were performed on a TGA V5.1A Dupont 2100 instrument from room temperature to 700 °C with a heating rate of 10 °C/min under flowing nitrogen. The emission/excitation spectra were recorded on a Hitachi 850 fluorescence spectrophotometer.

All gas sorption isotherms were measured using a Micromeritics ASAP 2020 M+C surface area and pore size analyzer. All the N₂, CO₂, and H₂ adsorption isotherms for desolvated **3** were collected in a relative pressure range from 10⁻⁴ to 1.0 atm. The cryogenic temperatures of 77 K required for N₂ and H₂ sorption measurements were controlled by liquid nitrogen, and the 273 K required for CO₂ was controlled using an ice–water bath. The initial outgassing process for the sample was carried out under a high vacuum (less than 10⁻⁶ mbar) at 90 for 10 h.

Synthesis of {[Ni(PA)(bpe)(H₂O)₂]·DMF}_n (1**)**. A mixture of H₂PA (0.030 g, 0.1 mmol), Ni(OAc)₂·6H₂O (0.026 g, 0.1 mmol), and *bpe* (0.008 g, 0.05 mmol) in H₂O (10 mL) was placed in a Parr Teflon-lined stainless steel vessel and heated to 120 °C for 72 h. Then the reaction system was cooled to room temperature slowly and green block crystals of **1** were obtained. After filtration, the crystals were washed with water and dried in air (0.024 g yield 32.5% based on H₂PA). C₃₈H₃₇N₃O₉Ni (738.42): calcd. C 61.76, H 5.01, N 5.69; found C 61.88, H 4.95, N 5.76. IR (KBr pellet): 3438(vs,br), 1632(m), 1613(m), 1553(w), 1509(w), 1459(s), 1385(m), 1353(m), 1236(w), 1204(w), 1094(w), 830(w), 742(w), 600(w), 556(m) cm⁻¹.

Synthesis of {[Zn(PA)(bpe)]·DMF}_n (2**)**. Procedures similar to those for **1** were performed to obtain colorless crystals of **2**, except that Zn(NO₃)₂·6H₂O was used instead of Ni(OAc)₂·6H₂O (0.028 g yield 39.5% based on H₂PA). C₃₈H₃₃N₃O₇Zn (709.04): calcd. C 64.31, H 4.65, N 5.92; found C 64.08, H 4.86, N 5.72. IR (KBr pellet): 3439(vs,br), 1618(s), 1509(m), 1452(vs), 1385(s), 1352(s), 1236(m), 1203(w), 1091(w), 1043(w), 825(s), 752(s), 696(w), 598(m), 562(m) cm⁻¹.

Synthesis of {[Zn(PA)(bpe)]·2DMF·CH₃OH}_n (3**)**. A solution of *bpe* (0.008 g, 0.05 mmol) in CH₃OH (3 mL) was carefully layered on a solution of Zn(NO₃)₂·6H₂O (0.025 g, 0.1 mmol) and pamoic acid (0.030 g, 0.10 mmol) in DMF (3 mL). Colorless single crystals of **3** were obtained in a few days (0.024 g yield 30.0% based on H₂PA). C₄₂H₄₄N₄O₉Zn (814.18): calcd. C 61.90, H 5.40, N 6.88; found C 62.04, H 5.18, N 6.88. IR (KBr pellet): 3437(s,br), 3056(w), 1631(s),

1612(s), 1508(w), 1446(m), 1384(m), 1361(m), 1234(w), 1042(w), 825(w), 752(w) cm⁻¹.

Synthesis of {[Cd₂(PA)₂(bpe)₂(H₂O)₂]·3.5H₂O}_n (4**)**. A mixture of H₂PA (0.030 g, 0.1 mmol), Cd(NO₃)₂·6H₂O (0.026 g, 0.1 mmol), and *bpe* (0.008 g, 0.05 mmol) in H₂O (10 mL) was placed in a Parr Teflon-lined stainless steel vessel and heated to 120 °C for 72 h. Then the reaction system was cooled to room temperature slowly and colorless block crystals of **4** were obtained. The crystals were filtrated, washed with water, and dried in air (0.022 g yield 30.6% based on H₂PA). C₁₄₀H₁₂₂N₈O₃₃Cd₄ (2894.06): calcd. C 58.04, H 4.21, N 3.87; found C 58.54, H 4.15, N 3.78. IR (KBr pellet): 3406(br), 3057(w), 2931(w), 1640(s), 1552(m), 1459(s), 1396(s), 1351(s), 1320(m), 1234(m), 1016(w), 831(m), 773(w), 547(w) cm⁻¹.

Synthesis of {[Ni₂(PA)(bpp)₂(H₂O)₃]·2DMF}_n (5**)**. Procedures similar to those for **1** were performed. *Bpp* was used instead of *bpe*. The reaction system was cooled to room temperature to give blue-green block crystals of **5** (0.032 g yield 43.0% based on H₂PA). C₇₈H₇₆N₆O₁₇·Ni₂ (1486.83): calcd. C 62.95, H 5.11, N 5.65; found C 62.88, H 5.03, N 5.52. IR (KBr pellet): 3436(vs,br), 1632(s), 1619(s), 1507(w), 1458(s), 1400(m), 1384(m), 1348(w), 1234(w), 1108(w), 756(w) cm⁻¹.

X-ray Crystallography. Suitable single crystals were selected for indexing, and intensity data were measured on a Siemens Smart CCD diffractometer with graphite-monochromated Mo Kα radiation ($\lambda = 0.71073 \text{ \AA}$) at 298 K. The raw data frames were integrated into SHELX-format reflection files and corrected using SAINT program. Absorption corrections based on multiscan were obtained by the SADABS program. The structures were solved with direct methods and refined with full-matrix least-squares technique using the SHELXS-97 and SHELXL-97 programs, respectively.¹² Displacement parameters were refined anisotropically, and the positions of the H-atoms were generated geometrically, assigned isotropic thermal parameters, and allowed to ride on their parent carbon atoms before the final cycle of refinement. Basic information pertaining to crystal parameters and structure refinement is summarized in Table 1, and selected bond lengths and angles are listed in Table S1, Supporting Information. CCDC 806033 (**1**), 806035 (**2**), 806034 (**3**), 806036 (**4**), 806037 (**5**) contain the supplementary crystallographic data for this paper. These data can be obtained free of charge from The Cambridge Crystallographic Data Centre via www.ccdc.cam.ac.uk/data_request/cif.

In **1**, the lattice DMF molecules are disordered over two general positions with a site occupancy of 0.5. In **2**, methylene C atoms of *bpe* ligand are disordered over two general positions (C29/C29', C30/C30') which were refined isotropically with a site occupancy of 0.81/0.19. The lattice DMF molecules are disordered over two general positions and were refined isotropically with a site occupancy of 0.76/0.24. Oxygen atoms of one lattice DMF molecule (O8/O8') in **3** are disordered and were refined isotropically with the a site occupancy of 0.57/0.43. In **4**, Cd₂ centers and the coordinated water molecules O8 are disordered over two general positions and refined isotropically with a site occupancy of 0.5. The lattice H₂O molecules are disordered over two general positions (O9 and O10) with a site occupancy of 0.5. Crystals of **5** diffracted poorly and good data were not obtained in spite of several trials.

■ RESULTS AND DISCUSSION

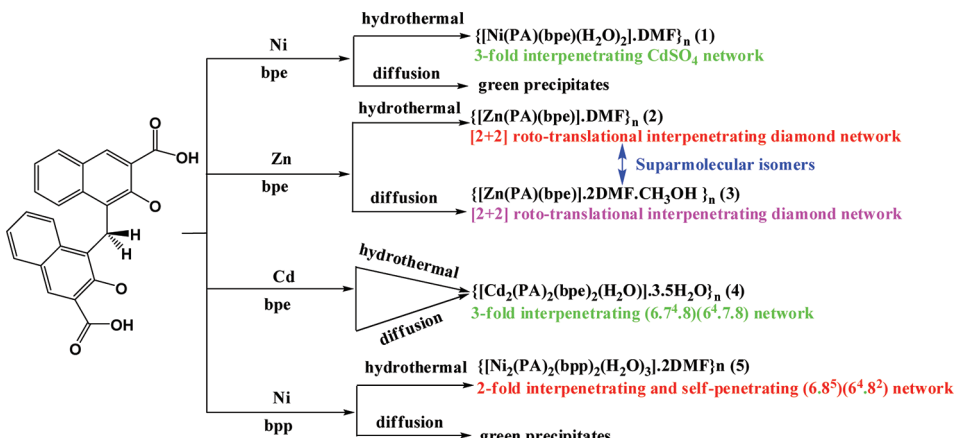
Syntheses of the Compounds. Reactions of the same starting materials were carried out through both hydrothermal and diffusion methods, respectively (Scheme 1). Interestingly, the resulting products were largely different for different systems. As shown in Scheme 2, **1** and **5** were only obtained hydrothermally. **2** and **3** were obtained through these two methods using the same starting materials. Both methods, however, could result into compound **4**. It seems that metal centers have effects on the products.

Table 1. Crystal Data and Structure Refinement Information for Compounds 1–5

compound	1	2	3	4	5
formula	C ₃₈ H ₃₇ N ₃ O ₉ Ni	C ₃₈ H ₃₃ N ₃ O ₇ Zn	C ₄₂ H ₄₄ N ₄ O ₉ Zn	C ₁₄₀ H ₁₃₃ N ₈ O ₃₃ Cd ₄	C ₇₈ H ₇₆ N ₆ O ₁₇ Ni ₂
formula weight	738.42	709.04	814.18	2894.06	1486.87
T (K)	298(2)	298(2)	298(2)	298(2)	298(2)
crystal system	monoclinic	orthorhombic	monoclinic	monoclinic	orthorhombic
space group	C ₂ /c	Pna ₂ 1	P2 ₁ /c	C ₂ /c	Iba ₂
a [Å]	19.469(6)	20.845(2)	13.6310(12)	25.102(2)	13.9830(12)
b [Å]	18.077(5)	13.0710(15)	17.3491(16)	13.6985(12)	29.496(3)
c [Å]	13.265(4)	12.4964(12)	20.2809(18)	20.929(2)	34.577(3)
α [°]	90.00	90.00	90.00	90.00	90.00
β [°]	131.213(4)	90.00	119.844(2)	107.745(2)	90.00
γ [°]	90.00	90.00	90.00	90.00	90.00
V [Å ³]	3512.0(17)	3404.9(6)	4160.1(6)	6854.4(11)	14261(2)
Z	4	4	4	2	8
D _{calcd} [g cm ⁻³]	1.397	1.383	1.300	1.402	1.385
μ [mm ⁻¹]	0.613	0.776	0.648	0.690	0.603
θ range	2.25–25.38	2.45–24.29	2.40–20.43	2.46–25.36	2.73–18.08
index ranges	−23 ≤ h ≤ 18 −21 ≤ k ≤ 16 −15 ≤ l ≤ 15	−18 ≤ h ≤ 24 −15 ≤ k ≤ 15 −14 ≤ l ≤ 14	−15 ≤ h ≤ 16 −20 ≤ k ≤ 20 −24 ≤ l ≤ 15	−29 ≤ h ≤ 29 −15 ≤ k ≤ 16 −24 ≤ l ≤ 13	−29 ≤ h ≤ 29 −15 ≤ k ≤ 16 −24 ≤ l ≤ 13
R ₁ , wR ₂ ^a [I > 2σ(I)]	0.0539; 0.1342	0.0493; 0.0974	0.0612; 0.1567	0.0911; 0.2090	0.1815; 0.4329
GOF	1.085	1.072	1.028	1.058	1.365

^a R₁ = Σ ||F_o|| − |F_c|| / |F_o|. wR₂ = [Σw(ΣF_o² − F_c²)² / Σw(F_o²)²]^{1/2}.

Scheme 1. Syntheses of the Compounds

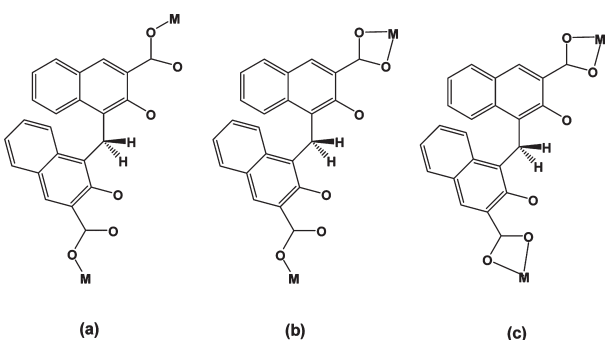


Structural Descriptions. {[Ni(PA)(bpe)(H₂O)₂]·DMF}_n (**1**). Compound **1** crystallizes in the space group C₂/c and the asymmetric unit consists of half of a Ni(II) ion, half PA²⁻ anion ligand, half bpe ligand, one coordinated aqua molecule, as well as half lattice DMF molecule (Figure 1). The Ni(II) ion lies on an inversion center, the PA²⁻ and bpe ligands lie about another independent inversion center, while the aqua molecule occupies a general position. The six-coordinated Ni(II) ion exhibits a slightly distorted octahedral geometry NiN₂O₄. The equatorial plane is composed of two carboxylate oxygen atoms from different PA²⁻ ligands and two nitrogen atoms of different bpe ligands, while two aqua molecules occupy the apical positions. The Ni—O and Ni—N distances in the equatorial plane are in the range of 2.048(3)–2.101(4) Å, and Ni—O distances in the apical positions are 2.083(3) Å, indicating the compressed octahedral environment of the metal ion.

The PA²⁻ and bpe ligand adopt bidentate (κ^1)-(κ^1)- μ_2 coordination mode and *anti* conformation, bridging the Ni(II) ions with the Ni1 \cdots Ni1A and Ni1 \cdots Ni1B (symmetry codes: A, 1 − x, y, 0.5 − z; B, 0.5 + x, 0.5 + y, 1 + z) distance of 15.90(6) and 13.50(3) Å, respectively. These two kinds of ligands are arranged in a slightly distorted planar arrangement around the metal centers, resulting into a three-dimensional network. The topological analysis reveals that it is a typical CdSO₄ framework the point symbol 6⁵.8 and the long symbol 6.6.6₂.6.6 with the Ni(II) center as planar 4-connected node. Three identical nets are further interpenetrating with each other, resulting into the final 3-fold network with each six-membered ring interpenetrating with other two six-membered rings.

In spite of even 3-fold interpenetration, one-dimensional channels are also generated in the compound. DMF molecules fill such

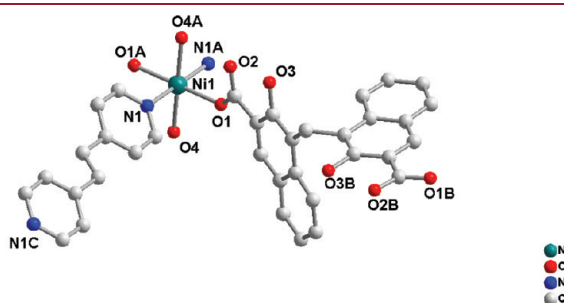
Scheme 2. Coordination Modes of the PA²⁻ Ligands in These Compounds^a



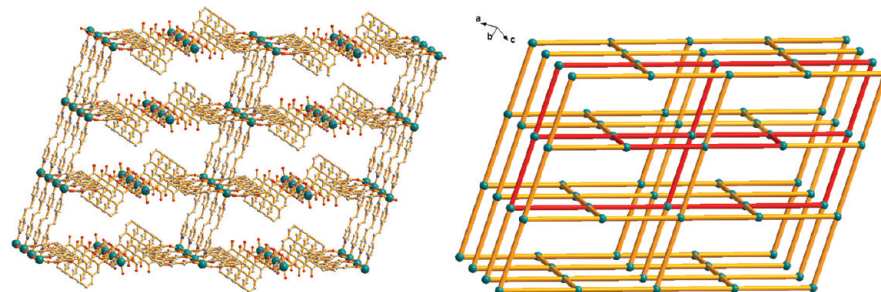
^a (a) (κ^1)-(κ^1)- μ_2 ; (b) (κ^1)-(κ^1 - κ^1)- μ_2 ; (c) (κ^1 - κ^1)-(κ^1 - κ^1)- μ_2 .

channels through hydrogen bonding interactions with the coordinated aqua molecules. The potentially accessible solvent volumes are 701.8 Å³, 20.0% in per unit as calculated by PLATON.¹³

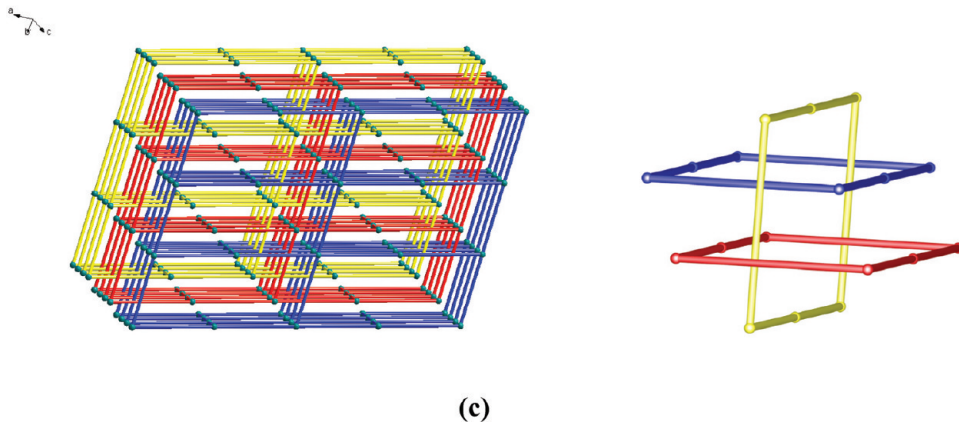
{[Zn(PA)(bpe)]·DMF}_n (**2**). Compound **2** crystallizes in the acentric space group *Pba*2₁ and exhibits unusual [2 + 2] diamond networks (Figure 2). The asymmetric unit is composed of one Zn(II) ion, one PA²⁻ ligand, one bpe ligand, as well as half disordered lattice DMF molecules. The Zn(II) ion is five-coordinated with one monodentate carboxylate oxygen atom and two chelating carboxylate oxygen atoms from two symmetry-related PA²⁻ ligands and two nitrogen atoms from two bpe ligands. The whole coordination geometry can be viewed as square pyramidal, with one nitrogen atom in the apical positions. The equatorial plane is much distorted with the mean deviation of 0.3539 Å with Zn(II) ions 0.3048 Å from the plane. The Zn—O and Zn—N bond distances fall in the range of 1.956–(6)–2.325(8) Å, respectively.



(a)



(b)



(c)

Figure 1. (a) The coordination environment of Ni(II) center in **1**. Symmetry code: A, 0.5 – x , 0.5 + y , –0.5 + z . (b) Left: Perspective of a single framework of **1**. Right: Topological representation of the CdSO₄ net. (c) Left: View of the 3-fold interpenetrating nets. Right: Scheme diagram of the polycatenane motif of **1**.

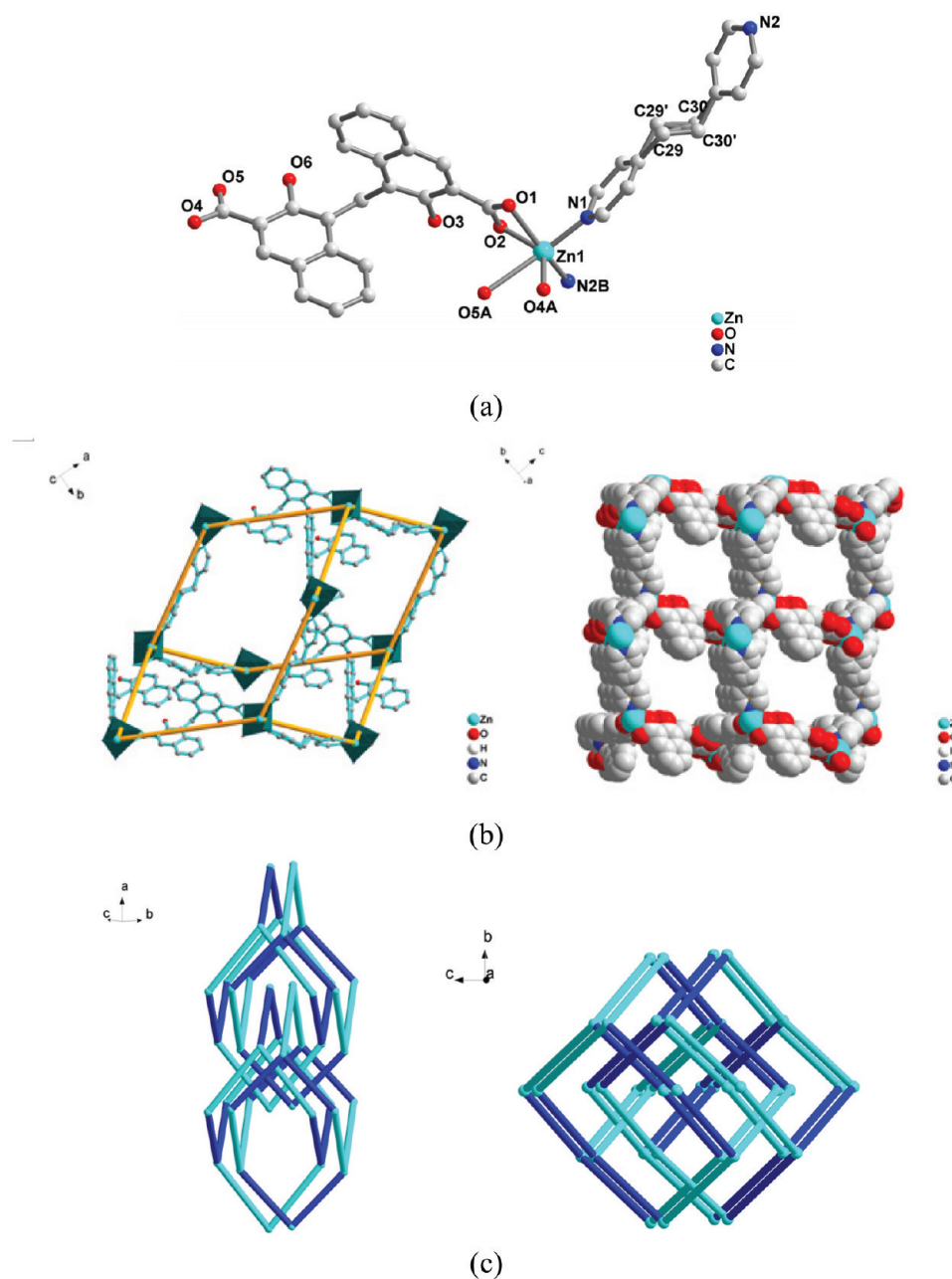


Figure 2. (a) The coordination environment of Zn(II) center in 2. Symmetry codes: A, $0.5 - x, 0.5 + y, -0.5 + z$; B, $-0.5 - x, 0.5 + y, 0.5 + z$. (b) Left: A single dia unit cage of 2. Right: The space filling mode of a single 3D dia net. (c) Left: Topological representation of the roto-translational [2 + 2] interpenetrating network of 2. Right: View of the interpenetrating nets approximately down the [0, 0, 1] direction. Light and deep blue sticks represent the connectivity of the metal centers through PA and bpe ligands, respectively.

The PA²⁻ and bpe ligand also adopt a bidentate (κ^1)-(κ^1 - κ^1)- μ_2 coordination mode and *anti* conformation with the Zn1 \cdots Zn1A and Zn1 \cdots Zn1B (symmetry codes: A, $1.5 - x, -0.5 + y, 0.5 + z$; B, $2.5 - x, -0.5 + y, -0.5 + z$) separation of 14.49(5) and 13.17(4) Å, respectively. Four of them in this case are in a tetrahedral arrangement around the Zn(II) center, leading to a three-dimensional (3-D) framework with the point symbol 6⁶ and the long symbol 6₂·6₂·6₂·6₂·6₂·6₂, typical of a diamondoid topology. The Zn \cdots Zn \cdots Zn angles are in the range 77.4(2) $-$ 125.8(2) $^\circ$, indicating a considerable distortion from the ideal tetrahedral angle of 109.8 $^\circ$. A single adamantanoid framework is illustrated in Figure 2b, which possesses maximum

dimensions (the longest intracage distances across the unit along the directions) of $41.69 \times 26.14 \times 24.99$ Å ($2a \times 2b \times 2c$). Such a large cavity causes four independent equivalent cages to interpenetrate with each other.

In a normal n -fold interpenetrating diamond net, the interpenetrating nets are related by the translation of $1/n$ of the diagonal distance across the adamantane unit along a shared 2-fold axis.¹⁴ The 4-fold interpenetrating net in this case, however, can be best described as two sets of a normal 2-fold net. Interestingly, the interpenetration vector in each set is the a axis, while the two sets are not translationally equivalent as the previously reported [$n + n$] modes,^{15,16} but related to a

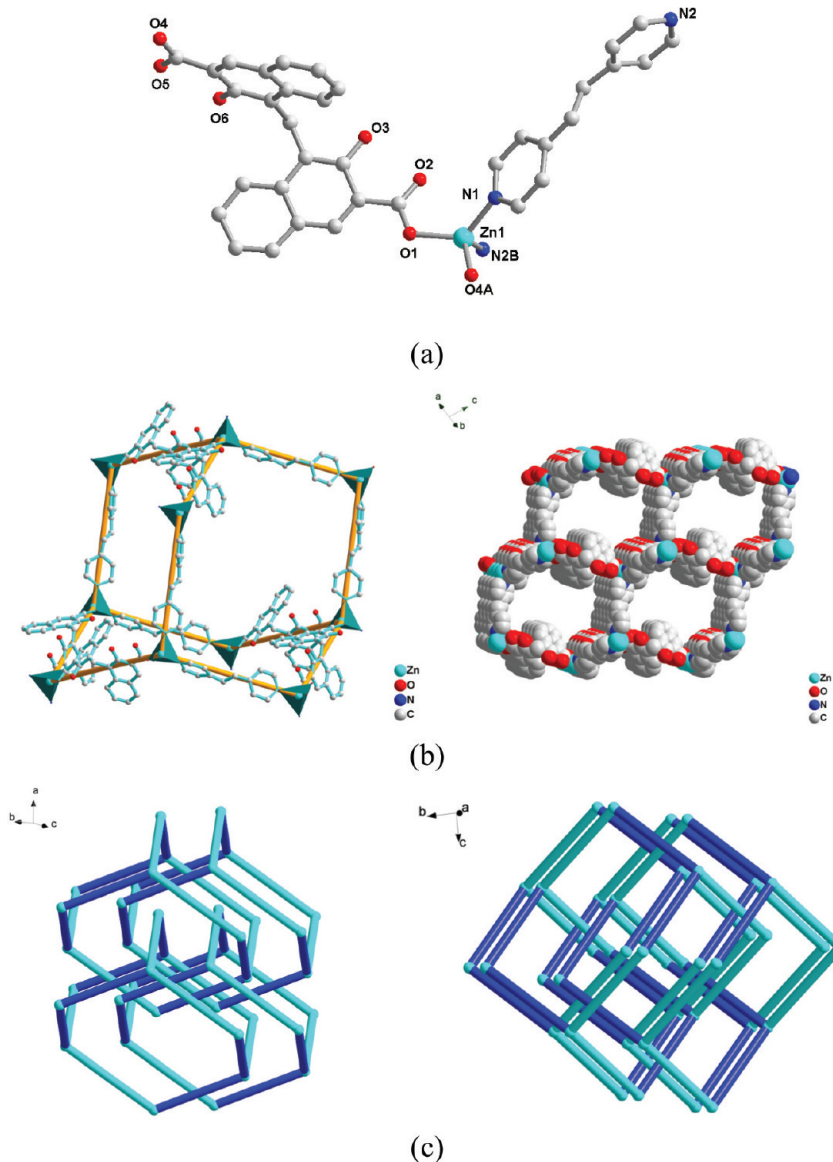


Figure 3. (a) The coordination environment of Zn(II) center in **3**. Symmetry codes: A, $0.5 - x, 0.5 + y, -0.5 + z$; B, $-0.5 - x, 0.5 + y, 0.5 + z$. (b) Left: A single dia unit cage of **3**. Right: The space filling mode of a single 3D dia net. (c) Left: Topological representation of the roto-translational [2 + 2] interpenetrating network of **3**. Right: View of the interpenetrating nets approximately down the [0, 0, 1] direction. Light and deep blue sticks represent the connectivity of the metal centers through PA and bpe ligands, respectively.

crystallographic 2-fold rotation parallel to the *b* direction. The second set is skewed to one side of the first one with a relative displacement of 6.32(3) Å. In another way, compound **2** is regarded as a [2 + 2] roto-translational interpenetrating diamondoid system (the class IIIa in RSCR notation)^{4e}. To the best of our knowledge, among those unusual interpenetrating examples, the roto-translational nets are very rare.¹⁷

In spite of even 4-fold interpenetration, one-dimensional channels are also generated in the compound, which are filled with DMF molecules, as evidenced by the elemental analysis and TGA data. The potentially accessible solvent volumes are 699.2 Å³ in per unit, 20.5%.

Structure of $\{[\text{Zn}(\text{PA})(\text{bpe})] \cdot 2\text{DMF} \cdot \text{CH}_3\text{OH}\}_n$ (3**)**. Compound **3** crystallizes in the space group $P2_1/c$. Although the PA²⁻ ligand adopts a bidentate (κ^1)-(κ^1)- μ_2 bridging mode and gives rise to a distorted square pyramidal geometry of Zn(II)

center, the whole net is also a diamondoid framework topologically (Figure 3). The 4-connected metal center exhibits a larger distortion from the ideal tetrahedral angle with the Zn···Zn distances and Zn···Zn···Zn angles in the range of 13.308(1)–15.076(1) Å and 99.278(6)–109.223(6)°, respectively. A single adamantanoid framework with maximum dimensions of 27.26 × 34.70 × 40.56 Å (2*a* × 2*b* × 2*c*) is illustrated in Figure 3a. Noticeably, this compound exhibits a similar roto-translational [2 + 2] interpenetration mode. The interpenetration vector in each set is also the *a* axis, while the two sets are related to a crystallographic 2-fold rotation parallel to the *c* direction with a relative displacement of 9.06(4) Å.

More interestingly, although the abnormal interpenetration also generates the channels, the sizes are much larger with the potential accessible solvent volumes of 1612.3 Å³ in per unit, 38.8% of the total unit. Significantly, interpenetration modes

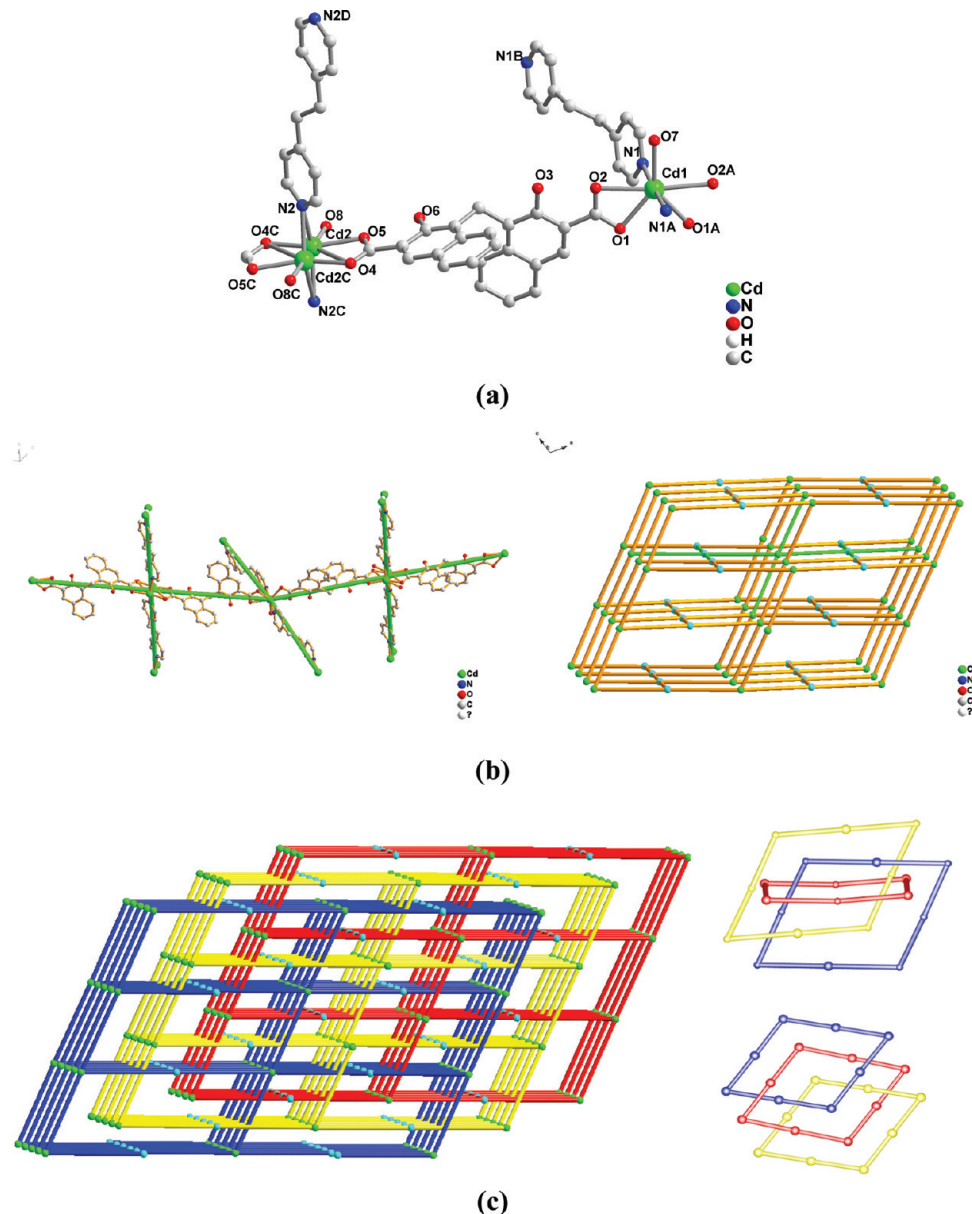


Figure 4. (a) The coordination environment of Cd(II) center in **4**. Symmetry code: A, $-x, +y, 1.5 - z$; B, $0.5 - x, 1.5 - y, 2 - z$; C, $1 - x, 1 - y, 1 - z$; D, $1 - x, 2 - y, 1 - z$. (b) Left: Perspective view of the connectivity of adjacent 4-connected planar nodes. Right: Topology of a single framework of **4**. (c) Left: Topological representation of the novel 4-connected net. Right: View of the 3-fold interpenetrating nets. Scheme diagram of the polycatenane motif of **4**.

have effects on the resulting porous structures, which are also largely dependent upon the weak interactions between the interpenetrating nets.

Fascinatingly, compounds **2** and **3** can be viewed as catenation-induced pseudosupramolecular isomers, which are generally related to the occurrence of interpenetration and non-interpenetration for a certain polymeric motif, or to the different interpenetrating/interweaving modes and degrees.¹⁸ To the best of our knowledge, supramolecular isomerism caused by diamondoid networks with [2 + 2] roto-translational interpenetration was found for the first time. Meanwhile, it should be noticeable that this may be one of the few supramolecular isomers with the two polymorphs exhibiting centrosymmetric or acentric coordination networks, respectively.¹⁹

$\{[Cd_2(PA)_2(bpe)_2(H_2O)] \cdot 3.5H_2O\}_n$ (**4**). Compound **4** crystallizes in the space group $C2/c$. The asymmetric unit consists of

one and one-half Cd(II) ions, one PA^{2-} ligand, half each of two bpe ligands (bpe-1, N1; bpe-2, N2), as well as two half coordinated aqua molecules and one-half and two quarter lattice aqua molecules (Figure 4). The Cd1 atom and PA^{2-} ligand lie at general positions while Cd2 and the two half bpe ligands lie about other independent inversion centers. The coordinated and the lattice water molecules also occupy general positions. The coordination geometry of Cd1 center can be described as pentagonal bipyramidal. The equatorial plane is composed of four chelating carboxylate oxygen atoms of different PA^{2-} ligands and one aqua molecule. The apical positions are situated by two nitrogen atoms from two bpe moieties. Cd2 center is disordered at two positions and adopts six-coordinated octahedral geometry. The equatorial is composed of two chelating carboxylate oxygen atoms, one monodentate carboxylate oxygen

atom of discrete PA²⁻ ligands, and one aqua molecule. The apical positions are occupied by two nitrogen atoms of two bpp ligands. The O–Cd–O angle in the equatorial plane and N–Cd–N angle along the apical direction are in the range of 50.8–149.4°, indicating the octahedron is much distorted.

The PA²⁻ ligands in bidentate ($\kappa^1\text{-}\kappa^1$)-($\kappa^1\text{-}\kappa^1$)- μ_2 coordination mode connect Cd1 and Cd2 alternately, resulting into one-dimensional chains with a Cd1···Cd2 distance of 15.47(6) Å. Two kinds of bpp ligands only bridge Cd1 or Cd2 centers, leading to two kinds of chains with Cd1···Cd1A and Cd2···Cd2B (symmetry codes: A, 0.5 - x , 1.5 - y , 2 - z ; B, 1 - x , 2 - y , 1 - z) distances of 13.72(5) and 13.78(6) Å, respectively. Three kinds of chains are not parallel but form angles about 90° with each other. Because of the disorder of Cd2 atoms, the centers of them and Cd1 atoms are viewed as nodes, which are all 4-connected nodes surrounded by two PA²⁻ ligands and two bpp ligands. For Cd1 nodes, the Cd···Cd···Cd angles are in the range 67.7(2)–114.2(7)°, indicating a slight distortion from the ideal plane. The Cd···Cd···Cd angles around Cd2 nodes, however, are in the range 79.3(2)–100.7(1)°, and the nodes are almost in the same plane. As a result, the whole net is a novel binodal 4-connected topology with the point symbol (6.7⁴.8)(6⁴.7.8) and the long symbol of 6₂.23₂.7₂.7₂.7₂ and 6.6.6.6.7₂, respectively. The net is related to the common topology of CdSO₄ (6⁵.8) and may be viewed as much distortion of the CdSO₄ net caused by the distortion of the geometry of the planar nodes. To the best of our knowledge, this novel topology is unprecedented in metal–organic chemistry. Three identical nets interpenetrate with each other, resulting in a 3-fold interpenetrating network.

{[Ni₂(PA)₂(bpp)₂(H₂O)₃]·2DMF}_n (**5**). Compound **5** is much more complicated. It crystallizes in the space group *Iba*2. The asymmetric unit is composed of two crystallographically independent Ni(II) centers, two PA²⁻ ligands (PA-1, O1–O6; PA-2, O7–O12), two bpp molecules (bpp-1, N1/N2; bpp-1, N3/N4) as well as three coordinated water molecules and two lattice DMF molecules (Figure 5). Ni1 and Ni2 centers adopt a similar distorted octahedral geometry with {NiO₄N₂} coordination environment while the coordinated atoms are slightly different. For Ni1, the equatorial plane is composed of one monodentate carboxylate oxygen atom, two chelating oxygen atoms of another PA²⁻ ligand, and one nitrogen atom of bpp ligand. One water molecule and one nitrogen atom of another bpp occupy the axial positions. For Ni2, however, the arrangement is totally different with two oxygen atoms from monodentate carboxyl groups of discrete PA²⁻ moieties situated at the axial positions and two nitrogen atoms of different bpp and two aqua oxygen atoms in the equatorial plane. Two aqua molecules are in the *cis* positions. The Ni–O and Ni–N distances and the angles are all consistent with the reported document.

The PA²⁻ ligands adopt a bidentate ($\kappa^1\text{-}\kappa^1$)-($\kappa^1\text{-}\kappa^1$)- μ_2 and ($\kappa^1\text{-}\kappa^1$)- μ_2 coordination mode and bridge Ni1 or Ni2 centers to form one-dimensional chains along the *a* and *b* axis with the Ni1···Ni1A and Ni2···Ni2B (symmetry codes: A, 1.5 - x , 0.5 + y , z ; B, 1 + x , y , z) distances of 15.12(3) and 13.98(4) Å, respectively. While two kinds of bpp ligands demonstrate *gauche-gauche* and *anti-gauche* conformations, bridging Ni1 and Ni2 centers alternately, giving rise to one-dimensional zigzag chains along the *c* axis. The Ni1···Ni2 and Ni1···Ni2C (symmetry code: C, - x , y , -0.5 + z) separations are 12.58(5) and 12.52(5) Å, respectively. The resulting 3-D architecture is formed by three kinds of chains sharing the metal centers.

Topologically, Ni1 and Ni2 centers are all surrounded by two PA²⁻ and two bpp ligands, which can be viewed as 4-connected

nodes with different geometries. Each Ni1 node is connected with two Ni1 and two Ni2 nodes with the Ni···Ni distances and adjacent Ni···Ni···Ni angles in the range 12.519(2)–13.983 Å and 45.2–180.0°, respectively, indicating a slight distortion from the ideal planar square. Each Ni2 node, however, is bridged with two Ni1 and two Ni2 nodes. The Ni···Ni distances and adjacent Ni···Ni···Ni angles are in the range 12.519(2)–15.116(2) Å and 87.0–154.6°, respectively, indicating a considerable distortion from the ideal tetrahedron. As a consequence, the whole net is constructed by equal mixed distorted planar and tetrahedral nodes with point symbol of (6.8⁵)(6⁴.8²) and long symbol of 6₂.8₂.8₂.8₂.8₂ and 6.6.6.6.8₂.9₆, respectively. It looks that the tetrahedral nodes have the same short point symbol as the NbO- and quartz-like net (6⁴.8²). However, they can be distinguished by their vertex symbols. The vertex symbols for the NbO- and quartz-like nets are 6₂.6₂.6₂.6₂.8₂.8₂ and 6.6.6₂.6₂.8₇.8₇, respectively. It is known that the majority of four-connected nets are constructed of square-planar or tetrahedral nodes. The former favors the generation of NbO (6⁴.8²-a), CdSO₄ (6⁵.8), lvt (4².8⁴), and quartz dual (7⁵.9) nets, and the latter would typically lead to quartz (6⁴.8²-b), diamond (6⁶) and sra (4².6³.8-a) nets.²⁰ The combination of both nodes is less reported, which is dependent upon the nodes ratio of 1:1 (pts) or 2:1 (mog), respectively.²¹ The current framework represents, as far as we know, an unprecedented case of such mixed nodes.

If the three types of links of different lengths were removed one at a time, a better insight into the nature of this intricate architecture is achieved (Figure 6). Elimination of one kind of bpp ligand (bpp-1 or bpp-2) leaves a 2-D 2-fold 2D → 2D parallel interpenetrating three-connected frame based on distorted triangular nodes. It has the point symbol [short (8².10) and long (8₂.8₂.∞)]. On moving one type of PA²⁻ ligand (PA-1), the remainders are 2-D (4,2)-connected layers. While if another kind of PA²⁻ ligand (PA-2) was moved, the remainders are 3-D (4,2)-connected frame based on planar and linear nodes, exhibiting an intriguing 6-fold interpenetrating substructure. If the linear nodes are omitted from topological view, each single net can be viewed as a 4-connected topology with point symbol (6⁵.8) and the long symbol of 6₂.6₂.6₂.6₂.∞, which is a novel net different from typical CdSO₄. Interestingly, this 6-fold interpenetration mode is also roto-translational with two sets of a normal 3-fold net related by a crystallographic 2-fold rotation parallel to the *a* direction. As a result of the unique bridging, the catenated eight-membered rings are observed; that is, each 8-membered ring is interlocked with two others of different sizes at one time. At the same time, two such nets interpenetrate with each other (Figure 7). Therefore, the resulting array is a rare 4-connected network with both self-penetration and interpenetration.

Carlucci et al. have previously reported a similar binodal 4-connected compound, [Cu(bpe)₂(SO₄)]·5H₂O (bpe = 1,2-bis(4-pyridyl)ethane), which possesses the same short point symbol.²² However, these two structures are largely different: compound **5** exhibits not only self-penetration but also 2-fold interpenetration, while the previous example is a single self-penetrating structure. Moreover, these two compounds possess different self-penetration modes: in a single structure of compound **5** only 8-rings are interlocked, while in the example all the basic circuits (six- and eight-membered rings) are catenated by other circuits. As far as we know, only several examples have been documented to display structural features of both interpenetration and self-penetration.²³

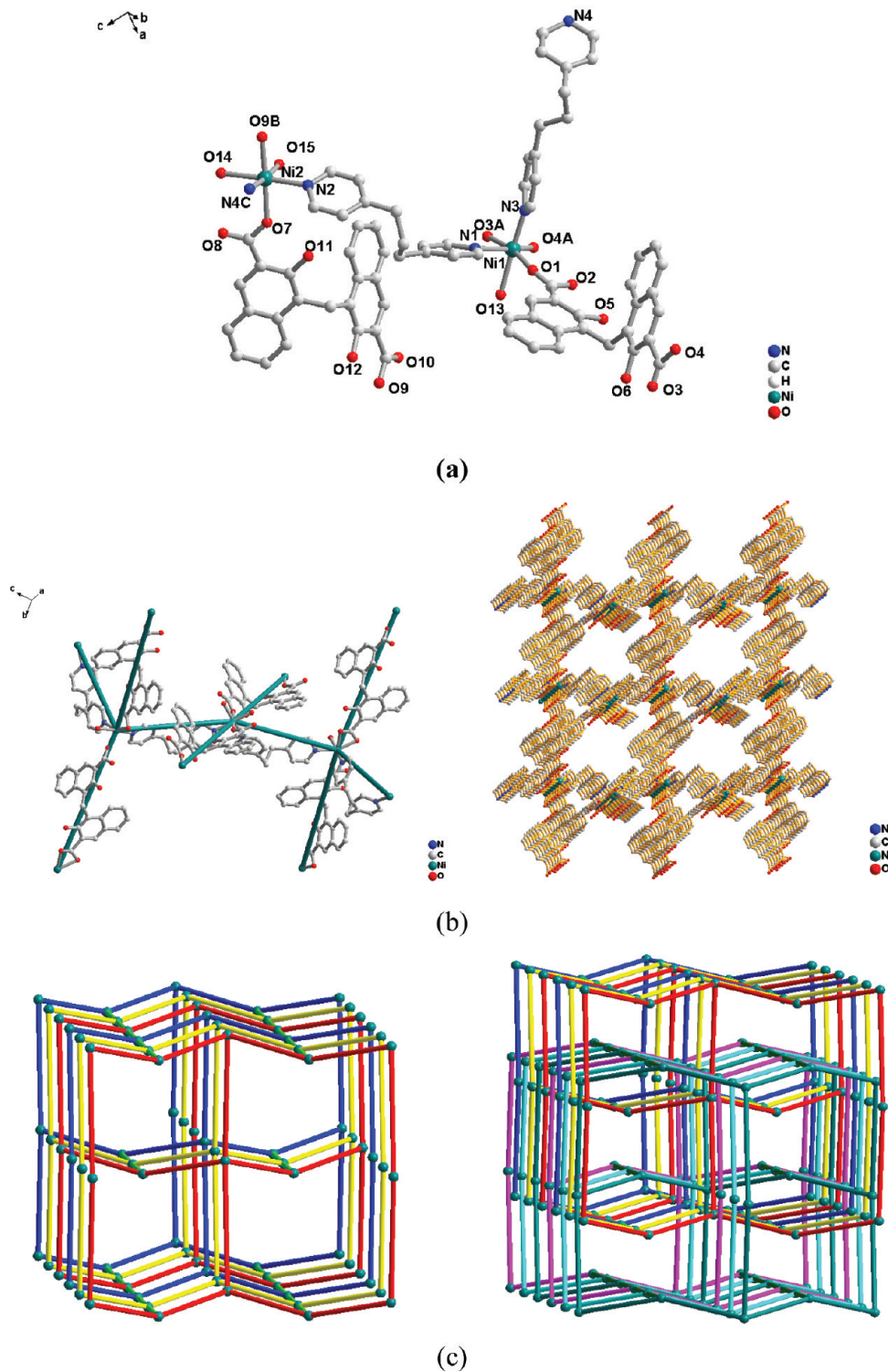


Figure 5. (a) The coordination environment of Ni(II) center in **5**. Symmetry code: A, $1.5 - x, 0.5 + y, z$; B, $1 + x, y, z$; C, $-x, y, 0.5 + z$. (b) Left: Perspective view of the connectivity of adjacent 4-connected nodes. Right: Perspective of a single framework of **5**. (c) Left: Topological representation of the novel 4-connected net. Right: View of the 2-fold interpenetrating nets.

■ DISCUSSION OF THE STRUCTURES

All of the five compounds exhibit penetrating characteristics, and the penetration modes are diverse and interesting, especially that of compound **5** which shows both interpenetration and self-penetration. Generally, the penetrating structures contain long

flexible ligands due to the fact that nature contrives to fill the “empty” space with the interpenetration models. As a result, the incorporation of polycarboxylates with flexible long-chain ligands is feasible for generating the entangled nets, and the degree of interpenetration is strongly related to the length of the spacer

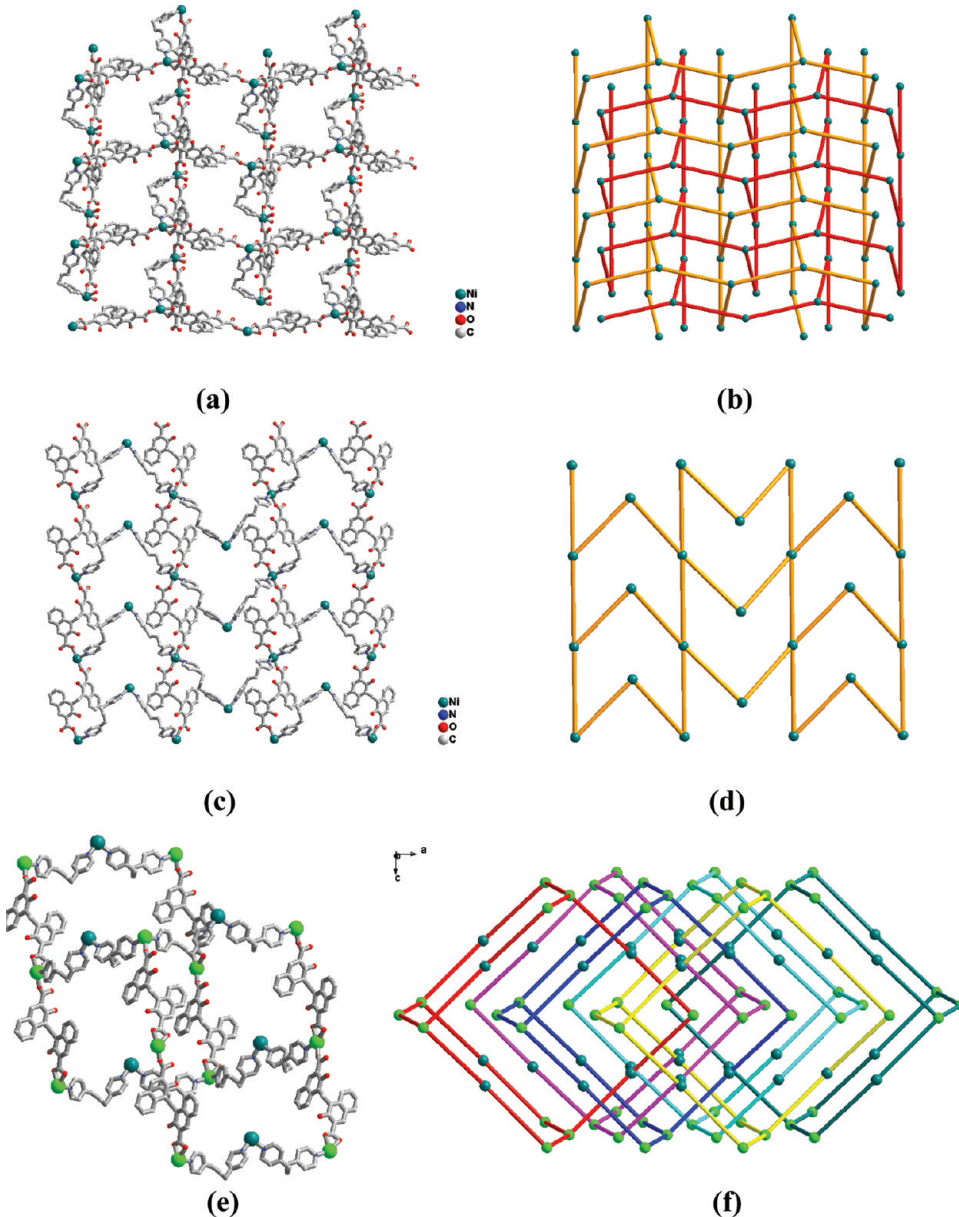


Figure 6. A rationalization of the topology of the network in **5**: In (a) the removal of bpe-1 or bpe-2 leads to two-dimensional three-connected layers that show $2D \rightarrow 2D$ parallel interpenetration, as schematically illustrated in (b); in (c) and (d) one can see the result of eliminating PA-1, which leaves two-dimensional layers only, extending in the *ac* plane; in (e) the elimination of PA-2 gives three-dimensional frameworks with the 4-connected ($\delta^3.8$) topology, which interpenetrate $[3 + 3]$ fold as schematically shown in (f).

ligand. The H_2PA ligand is a semirigid dicarboxylate ligand containing the $-CH_2-$ groups and may adopt many conformations, including those symmetrical and asymmetrical. Depending on the coordination requirement of the metal center and a particular network formation, the ligand can adopt different conformations via bending, stretching, or twisting. The flexible bpe and bpp ligand can also exhibit different conformations with respect to the relative orientations of the $-CH_2-$ groups. These ligands could cooperate with each other by adjusting their conformations to generate coordination diversity of the metal centers and further the geometry of the metal nodes. A superimposed picture of the ligands in the compounds will put this into perspective (Table 2 and Figure 8). The conformational variations can broadly be quantified by several parameters:

(i) the dihedral angles of two naphthalate rings; (ii) *anti* or *gauche* conformation of the bpe or bpp ligands; (iii) dihedral angles of two pyridyl rings. It can be seen that metal \cdots metal separations by these ligands are in the range of $12.52(5)$ – $15.90(5)$ Å. Such large distances of course easily cause the penetration.

Of course, other factors also affect interpenetration, such as the bulkiness of the ligands and the counterions, the type and number of solvated molecules, the $\pi \cdots \pi$ or $C-H \cdots \pi$ interactions between the aromatic bridging ligands, the coordination geometry of the metal centers, and so on. Further investigations on the weak interactions in these compounds demonstrate that weak aromatic interactions are observed between the naphthalate and pyridyl groups or within both groups (Figure S1-5, Supporting Information). The diverse penetration modes may be related with

the ways and strengths of these interactions. Anyway, these special structures may enrich the frameworks of multicarboxylate systems to some extent.

Thermogravimetric Analysis and Gas Adsorption Studies. The XRPD measurement shown that the diffraction peaks of both the simulated and experimental patterns match well in relevant positions, indicating the phase purities of these compounds (Figure S6, Supporting Information). Thermogravimetric analysis (TGA) was performed on compounds **1–5** to investigate the thermal stability of these polymers (Figure S7, Supporting Information). The TGA curve of compound **1** displays steady weight loss in the temperature range 100–230 °C (found: 10.5%), corresponding to the evacuation of the lattice DMF molecules (calc. 9.9%). The decomposition of the whole structure corresponds to the rapid weight loss in 290–390 °C. For compound **2**, the loss of the lattice DMF molecules (calc. 10.3%) occurs in 180–230 °C (found: 9.7%), and the rapid

weight loss in the temperature range 295–375 °C indicates the decomposition of the structure. Because of the large cavity of compound **3**, the comparably large weight loss from 60 to 190 °C corresponds to the evacuation of the lattice DMF and CH₃OH molecules (found: 20.5%, calc. 21.8%). No weight loss occurred until approximately 330 °C, indicating the decomposition of the whole structure from then on. No weight loss occurred until approximately 330 °C, indicating the decomposition of the whole structure from then on. TGA of compound **4** reveals a steady weight loss between 150 and 190 °C, which is attributed to the loss of the lattice water molecules (found 3.1%, calc'd 2.5%). The whole network began to decompose from approximately 300 °C. Compound **5** exhibits several steps of weight loss, the first of which begins at 225 °C and ends at 255 °C. During this in the temperature range, the lattice DMF molecules are lost (found 10.1%, calc'd 9.8%). From then on, the whole network began to decompose.

In order to evaluate the porosity of these compounds, gas sorption measurements were carried out. Fresh samples were first solvent exchanged with CH₂Cl₂ and then outgassed at 90 °C for 10 h under a vacuum. Unfortunately, only compound **3** showed adsorptive activities in spite of 4-fold interpenetration (Figure S8, Supporting Information). The activated sample hardly adsorbs N₂ gas (8.0 cm³·g⁻¹ before 700 Torr) at 77 K but reveals a moderate absorption of H₂ (16.8 cm³·g⁻¹, 0.15 wt % at 700 Torr). The rare large hysteresis of the hydrogen sorption isotherms may be related to both the small apertures and the amounts of rings of PA²⁺ ligands by increasing the synergistic effect of the neighboring pore walls and accordingly slow the adsorption kinetics.²⁴ Moreover, with the flexible and interpenetrative of the framework, the activated sample exhibits adsorption for CO₂ up to 3.78 wt % (19.3 cm³·g⁻¹) at 273 K and 800 Torr. This selective adsorption behavior has also been found

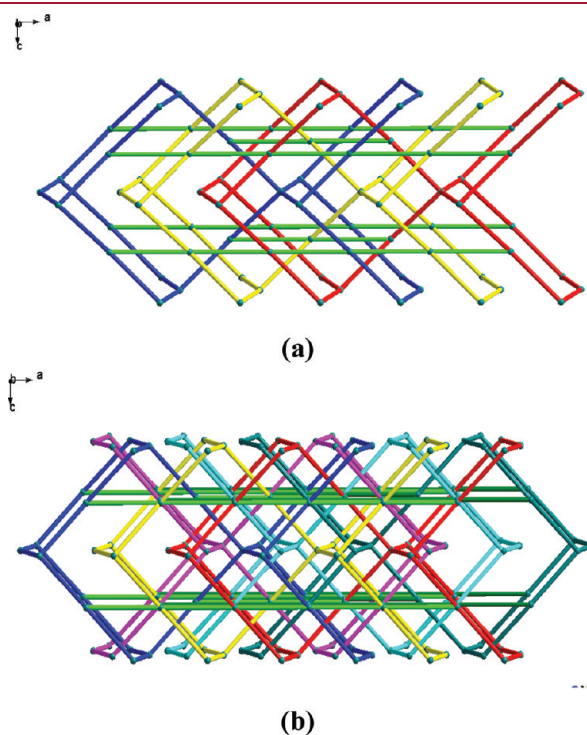


Figure 7. (a) The 4-connected self-penetrating net derived from three interpenetrating nets in **5**. (b) View of the 2-fold interpenetrating mode of each single self-penetrating net.

Table 2. Conformation of PA²⁺ and Dipyridyl Ligands, Dihedral Angles of Two Naphthalene Rings of PA Ligands and Pyridine Rings, M···M Separation between Two Carboxylate Groups and Two Donor N Atoms in Compounds **1–5**

compound	coordination mode of the PA ²⁺ ligand	dihedral angles of two naphthalene rings (deg)	M...M distance separated by PA ²⁺ ligand (Å)	bpe or bpp conformation	M···M distance separated by bpea/bpp ligand (Å)	dihedral angles of two pyridyl rings (deg)
1	bidentate (κ^1)-(κ^1)- μ_2	136.7	15.90(5)	anti	13.50(2)	0
2	bidentate (κ^1)-(κ^1 - κ^1)- μ_2	94.1	15.10(2)	anti	13.30(2)	27.8
3	bidentate (κ^1)-(κ^1)- μ_2	97.8	15.07(1)	anti	13.31(1)	78.5
4	bidentate (κ^1 - κ^1)-(κ^1 - κ^1)- μ_2	79.8	15.08(2)	anti	13.70(2)	0
5	bidentate (κ^1)-(κ^1 - κ^1)- μ_2 and (κ^1)-(κ^1)- μ_2	86.1 65.1	15.12(3) 13.98(4)	gauche-gauche and anti-gauche	12.58(5) 12.52(5)	117.7 92.3

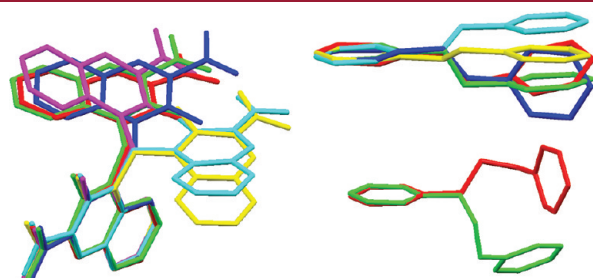


Figure 8. Overlay of pamoate, bpe, and bpp moieties in the five compounds.

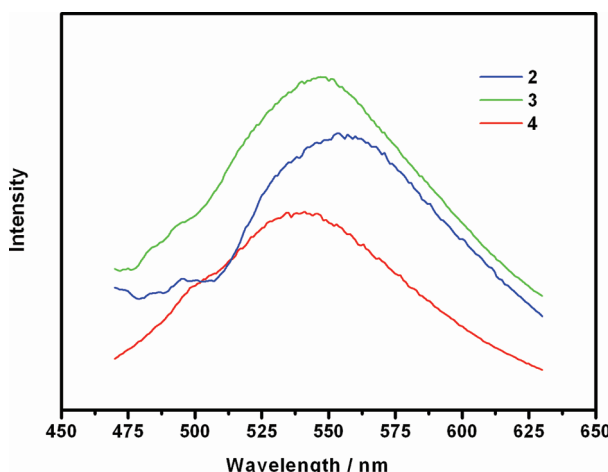


Figure 9. Photoluminescence properties of **2–4**.

in other reported coordination polymers and could also be attributed to the small apertures of the channels that prevent the entrance of N_2 (kinetic diameter: 3.64 Å) but allow the diffusion of CO_2 (kinetic diameter: 3.30 Å) and H_2 (kinetic diameter: 2.89 Å) into the channels.²⁵ The gas uptakes are not as high as the pore volume based upon the crystal structure, which may be derived from the partial collapse or shrinkage of the framework of compound **3** after removal of the guests.

Photoluminescent and SHG Properties. Inorganic–organic hybrid coordination complexes, especially with d^{10} metal centers, have been investigated for fluorescence properties owing to their potential applications as luminescent materials.²⁶ The photoluminescence spectra of the pamoic acid and compounds **2–4** were measured in the solid state at room temperature (Figure 9). The photoluminescent spectrum of pamoic acid has been investigated and shows the emission maxima at 474 nm with the excitation at 434 nm, which may be attributable to the intraligand $\pi \rightarrow \pi^*$ transitions.^{11a} The similar and significant redshifts of emission bands of the metal compounds (554 nm with $\lambda_{\text{ex}} = 424$ nm for **2**, 547 nm with $\lambda_{\text{ex}} = 420$ nm for **3**, 538 nm with $\lambda_{\text{ex}} = 420$ nm for **4**) should be ascribed to neither metal-to-ligand charge transfer (MLCT) nor ligand-to-metal charge transfer (LMCT) in nature because the Zn(II) and Cd(II) ions are difficult to oxidize or to reduce. Consequently, the emission could be assigned to the intraligand transitions.²⁷ The difference of the intensity may result from different metal centers and conformational ligands as well as weak interactions in the interpenetrating crystalline lattice, which may affect the rigidity of the whole network and further the energy transfer involved in the luminescence.²⁸

To confirm the acentricity of compounds **2** and **5**, quasi-Kurtz SHG measurements on the powder samples of them have been performed. Preliminary experimental results show that the bulk materials for these compounds display powder SHG efficiencies of approximately 0.3 and 0.4 times that of urea.

■ CONCLUSION

On the basis of pamoic acid, five novel compounds have been synthesized through hydrothermal or diffusion methods. Because of diverse coordination modes and conformations of the semirigid dicarboxylate ligand and pyridyl-containing coligands, these compounds exhibit diverse 4-connected topologies with

interesting entangled modes: 3-fold interpenetrating CdSO_4 net ($6^5.8$) (**1**), roto-translational [2 + 2] interpenetrating diamond pseudosupramolecular isomers (**2** and **3**), 3-fold interpenetrating ($6.7^4.8$)($6^4.7.8$) net (**4**), and (6.8^5)($6^4.8^2$) net with both 2-fold interpenetrating and self-penetrating characters (**5**), respectively. The formation of unique penetrating frameworks was investigated in detail. Gas adsorption, photoluminescence, and SHG properties of the compounds have also been performed. In summary, our research demonstrates that the pamoic acid could act as a potential building block with the combination of different coligands to construct novel supramolecular architectures with unusual entangled topologies and properties.

■ ASSOCIATED CONTENT

S Supporting Information. Additional figures, TGA, and gas adsorption curves of the compounds. This material is available free of charge via the Internet at <http://pubs.acs.org>.

■ AUTHOR INFORMATION

Corresponding Author

*E-mail: jmdou@lcu.edu.cn (J.B.), bjunfeng@nju.edu.cn (J.D.).

■ ACKNOWLEDGMENT

We gratefully acknowledge financial support from the National Natural Science Foundation of China (Grant Nos. 20801025 and 21001061) and Shandong Taishan Scholar Fund.

■ REFERENCES

- (a) Farha, O. K.; Hupp, J. T. *Acc. Chem. Res.* **2010**, *43*, 1166.
- (b) Liu, Y.; Xuan, M. M.; Cui, Y. *Adv. Mater.* **2010**, *22*, 4112.
- (c) Tranchemontagne, D. J. L.; Mendoza-Cortes, J. L.; O’Keeffe, M.; Yaghi, O. M. *Chem. Soc. Rev.* **2009**, *38*, 1257.
- (d) Tranchemontagne, D. J. L.; Ni, Z.; O’Keeffe, M.; Yaghi, O. M. *Angew. Chem., Int. Ed.* **2008**, *47*, S136.
- (e) Ferey, G.; Mellot-Draznieks, C.; Serre, C.; Millange, F. *Acc. Chem. Res.* **2005**, *38*, 217.
- (f) Kitagawa, S.; Kitaura, R.; Noro, S. *Angew. Chem., Int. Ed.* **2004**, *43*, 2334.
- (g) Eddaoudi, M.; Moler, D. B.; Li, H. L.; Chen, B. L.; Reineke, T. M.; O’Keeffe, M.; Yaghi, O. M. *Acc. Chem. Res.* **2001**, *34*, 319.
- (2) (a) Zou, R. Q.; Abdel-Fattah, A. I.; Xu, H. W.; Zhao, Y. S.; Hickmott, D. D. *CrystEngComm.* **2010**, *12*, 1337. (b) Ma, L. Q.; Mihalcik, D. J.; Lin, W. B. *J. Am. Chem. Soc.* **2009**, *131*, 4610. (c) Jia, J. H.; Lin, X.; Wilson, C.; Blake, A. J.; Champness, N. R.; Hubberstey, P.; Walker, G.; Cussen, E. J.; Schroder, M. *Chem. Commun.* **2007**, 840.
- (d) Ma, S. Q.; Sun, D. F.; Ambrogio, M.; Fillinger, J. A.; Parkin, S.; Zhou, H. C. *J. Am. Chem. Soc.* **2007**, *129*, 1858.
- (e) Pan, L.; Olson, D. H.; Ciemolonski, L. R.; Heddy, R.; Li, J. *Angew. Chem., Int. Ed.* **2006**, *45*, 616.
- (f) Dybtsev, D. N.; Nuzhdin, A. L.; Chun, H.; Bryliakov, K. P.; Talsi, E. P.; Fedirn, V. P.; Kim, K. *Angew. Chem., Int. Ed.* **2006**, *45*, 916.
- (3) (a) Xu, J.; Bai, Z. S.; Chen, M. S.; Su, Z.; Chen, S. S.; Sun, W. Y. *CrystEngComm.* **2009**, *11*, 2728. (b) Li, Z. X.; Xu, Y.; Zuo, Y.; Li, L.; Pan, Q. H.; Hu, T. L.; Bu, X. H. *Cryst. Growth Des.* **2009**, *9*, 3904.
- (4) (a) Batten, S. R.; Robson, R. *Angew. Chem., Int. Ed.* **1998**, *37*, 1461. (b) Batten, S. R. *CrystEngComm.* **2001**, *3*, 67. (c) Carlucci, L.; Ciani, G.; Proserpio, D. M. *Coord. Chem. Rev.* **2003**, *246*, 247. (d) Blatov, V. A.; Carlucci, L.; Ciani, G.; Proserpio, D. M. *CrystEngComm* **2004**, *6*, 378. (e) Blatov, V. A.; Carlucci, L.; Ciani, G.; Proserpio, D. M. *CrystEngComm* **2004**, *6*, 377. (f) Baburin, I. A.; Blatov, V. A.; Carlucci, L.; Ciani, G.; Proserpio, D. M. *J. Solid State Chem.* **2005**, *178*, 2452.
- (5) (a) Baburin, I. A.; Blatov, V. A.; Carlucci, L.; Ciani, G.; Proserpio, D. M. *Cryst. Growth Des.* **2008**, *8*, 519. (b) Martin, D. P.; LaDuca, R. L. *Inorg. Chem.* **2008**, *47*, 9754. (c) Shyu, E.; Supkowski, R. M.; LaDuca,

- R. L. *Inorg. Chem.* **2009**, *48*, 2723. (d) Ke, X. J.; Li, D. S.; Du, M. *Inorg. Chem. Commun.* **2011**, *14*, 788.
- (6) (a) Li, D. S.; Ke, X. J.; Zhao, J.; Du, M.; Zou, K.; He, Q. F.; Li, C. *CrystEngComm* **2011**, *13*, 3355. (b) Ma, L. Q.; Wu, C. D.; Wanderley, M. M.; Lin, W. B. *Angew. Chem., Int. Ed.* **2010**, *49*, 8244. (c) Liang, L. L.; Ren, S. B.; Zhang, J.; Li, Y. Z.; Du, H. B.; You, X. Z. *Dalton Trans.* **2010**, *39*, 7723. (d) Su, Z.; Fan, J.; Okamura, T. A.; Chen, M. S.; Chen, S. S.; Sun, W. Y.; Ueyama, N. *Cryst. Growth Des.* **2010**, *10*, 1911. (e) Li, D. S.; Fu, F.; Zhao, J.; Wu, Y. P.; Du, M.; Zou, K.; Dong, W. W.; Wang, Y. Y. *Dalton Trans.* **2010**, *39*, 11522. (f) Ma, L. F.; Wang, L. Y.; Wang, Y. Y.; Batten, S. R.; Wang, J. G. *Inorg. Chem.* **2009**, *48*, 915. (g) Feng, R.; Jiang, F. L.; Chen, L.; Yan, C. F.; Wu, M. Y.; Hong, M. C. *Chem. Commun.* **2009**, *35*, 5296.
- (7) (a) Yao, S. Y.; Tian, Y. Q. *CrystEngComm* **2010**, *12*, 697. (b) Ma, L. F.; Meng, Q. L.; Li, C. P.; Li, B.; Wang, L. Y.; Du, M.; Liang, F. P. *Cryst. Growth Des.* **2010**, *10*, 3036. (c) Qi, Y.; Che, Y. X.; Zheng, J. M. *Cryst. Growth Des.* **2008**, *8*, 3602. (d) Wang, X. L.; Qin, C.; Wang, E. B.; Su, Z. M. *Chem.—Eur. J.* **2006**, *12*, 2680. (e) Wang, X. L.; Qin, C.; Wang, E. B.; Su, Z. M.; Xu, L.; Batten, S. R. *Chem. Commun.* **2005**, 4789. (f) Li, X.; Cao, R.; Sun, D. F.; Bi, W. H.; Yuan, D. Q. *Eur. J. Inorg. Chem.* **2004**, 2228.
- (8) (a) Li, D. S.; Fu, F.; Zhao, J.; Wu, Y. P.; Du, M.; Zou, K.; Dong, W. W.; Wang, Y. Y. *Dalton Trans.* **2010**, *39*, 11522. (b) Tynan, E.; Jensen, P.; Kelly, N. R.; Kruger, P. E.; Lees, A. C.; Moubaraki, B.; Murray, K. S. *Dalton Trans.* **2004**, 3440. (c) Wen, L. L.; Lu, Z. D.; Lin, J. G.; Tian, Z. F.; Zhu, H. Z.; Meng, Q. J. *Cryst. Growth Des.* **2007**, *7*, 93. (d) Wang, H. L.; Zhang, D. P.; Sun, D. F.; Chen, Y. T.; Zhang, L. F.; Tian, L. J.; Jiang, J. Z.; Ni, Z. H. *Cryst. Growth Des.* **2009**, *9*, 5273.
- (9) (a) Feng, R.; Jiang, F. L.; Chen, L.; Yan, C. F.; Wu, M. Y.; Hong, M. C. *Chem. Commun.* **2009**, 5296. (b) Xu, J.; Bai, Z. S.; Chen, M. S.; Su, Zhi; Chen, S. S.; Sun, W. Y. *CrystEngComm* **2009**, *11*, 2728. (c) Habib, H. A.; Hoffmann, A.; Höpke, H. A.; Janiak, C. *Dalton Trans.* **2009**, 1742.
- (10) (a) Duan, J. G.; Bai, J. F.; Zheng, B. S.; Li, Y. Z.; Ren, W. T. *Chem. Commun.* **2011**, 2556. (b) Wang, S. N.; Xing, H.; Li, Y. Z.; Bai, J. F.; Scheer, M.; Pan, Y.; You, X. Z. *Chem. Commun.* **2007**, 2293. (c) Wang, S. N.; Bai, J. F.; Xing, H.; Li, Y. Z.; Song, Y.; Pan, Y.; Scheer, M.; You, X. Z. *Cryst. Growth Des.* **2007**, *7*, 747. (d) Wang, S. N.; Li, D. C.; Dou, J. M.; Wang, D. Q. *Acta Crystallogr.* **2010**, *C66*, m118.
- (11) (a) Du, M.; Li, C. P.; Zhao, X. J.; Yu, Q. *CrystEngComm* **2007**, *9*, 1011. (b) Wang, J. J.; Yang, M. L.; Hu, H. M.; Xue, G. L.; Li, D. S.; Shi, Q. Z. *Inorg. Chem. Commun.* **2007**, *10*, 269. (c) Shi, Q.; Sun, Y. T.; Sheng, L. Z.; Ma, K. F.; Hu, M. L.; Hu, X. G.; Huang, S. M. *Cryst. Growth Des.* **2008**, *8*, 3401. (d) Luo, F.; Yang, Y. T.; Che, Y. X.; Zheng, J. M. *CrystEngComm* **2008**, *10*, 981. (e) Du, M.; Zhang, Z. H.; Guo, W.; Fu, X. J. *Cryst. Growth Des.* **2009**, *9*, 1655. (f) Haynes, D. A.; Weng, Z. F.; Jones, W.; Motherwell, W. D. S. *CrystEngComm* **2009**, *11*, 254. (g) Shi, X. M.; Li, M. X.; He, X. A.; Liu, H. J.; Shao, M. *Polyhedron* **2010**, *29*, 2075.
- (12) (a) Sheldrick, G. M. *SHELXS-97, Program for Crystal Structure Solution*; Göttingen University: Göttingen, Germany, 1997. (b) Sheldrick, G. M. *SHELXL-97, Program for Crystal Structure Refinement*; Göttingen University: Göttingen, Germany, 1997.
- (13) Spek, A. L. *J. Appl. Crystallogr.* **2003**, *36*, 7.
- (14) (a) Zaworotko, M. J. *J. Chem. Soc. Rev.* **1994**, *23*, 283. (b) Batten, S. R.; Robson, R. *Angew. Chem., Int. Ed.* **1998**, *37*, 1460. (c) Evans, O. R.; Lin, W. *Acc. Chem. Res.* **2002**, *35*, 511. (d) Carlucci, L.; Ciani, G.; Proserpio, D. M.; Rizzato, S. *Chem.—Eur. J.* **2002**, *8*, 1520. (e) Kim, H.; Suh, M. P. *Inorg. Chem.* **2005**, *44*, 810. (f) Rood, J. A.; Noll, B. C.; Henderson, K. W. *Inorg. Chem.* **2006**, *45*, 5521.
- (15) (a) Shi, F. N.; Cunha-silva, L.; Trindade, T.; Almeida, P. F.; Rocha, J. *Cryst. Growth Des.* **2009**, *9*, 2098. (b) Hsu, Y. F.; Lin, C. H.; Chen, J. D.; Wang, J. C. *Cryst. Growth Des.* **2008**, *8*, 1094. (c) Giri, R.; Chen, X.; Yu, J. Q. *Angew. Chem., Int. Ed.* **2005**, *44*, 2115. (d) Kim, H.; Suh, M. P. *Inorg. Chem.* **2005**, *44*, 810. (e) Carlucci, L.; Ciani, G.; Proserpio, D. M.; Rizzato, S. *Chem.—Eur. J.* **2002**, *8*, 1520. (f) Xiong, R. G.; Zuo, J. L.; You, X. Z.; Abrahams, B. F.; Bai, Z. P.; Che, C. M.; Fun, H. F. *Chem. Commun.* **2000**, 2061.
- (16) (a) Xiao, D. R.; Li, Y. G.; Wang, E. B.; Fan, L. L.; An, H. Y.; Su, Z. M.; Xu, L. *Inorg. Chem.* **2007**, *46*, 4158. (b) Lee, H. Y.; Park, J.; Lah, M. S.; Hong, J. I. *Cryst. Growth Des.* **2008**, *8*, 587. (c) Ma, L. F.; Wang, Y. Y.; Liu, J. Q.; Yang, G. P.; Du, M.; Wang, L. Y. *CrystEngComm* **2009**, *11*, 1800.
- (17) (a) Chen, Z. F.; Xiong, R. G.; Abrahams, B. F.; You, X. Z.; Che, C. M. *Dalton Trans.* **2001**, 2453. (b) Westcott, A.; Whitford, N.; Hardie, M. J. *Inorg. Chem.* **2004**, *43*, 3663. (c) Baburin, I. A.; Blatov, V. A.; Carlucci, L.; Ciani, G.; Proserpio, D. M. *Cryst. Growth Des.* **2008**, *8*, 519.
- (18) (a) Ma, S. Q.; Sun, D. F.; Ambrogio, M.; Filinger, J. A.; Parkin, S.; Zhou, H. C. *J. Am. Chem. Soc.* **2007**, *129*, 1858. (b) Peng, R.; Li, M. A.; Deng, S. R.; Li, Z. Y.; Li, D. *CrystEngComm* **2010**, *12*, 3670. (c) Zhao, X. L.; He, H. Y.; Dai, F. N.; Sun, D. F.; Ke, Y. X. *Inorg. Chem.* **2010**, *49*, 8650. (d) Zhang, J. P.; Qi, X. L.; He, C. T.; Wang, Y.; Chen, X. M. *Chem. Commun.* **2011**, *47*, 4156. (e) Lee, J. Y.; Chen, C. Y.; Lee, H. M.; Passaglia, E.; Vizza, F.; Oberhauser, W. *Cryst. Growth Des.* **2011**, *11*, 1230.
- (19) (a) Li, Z. G.; Wang, G. H.; Jia, H. Q.; Hu, N. H.; Xu, J. W. *CrystEngComm* **2007**, *9*, 882. (b) Zhao, X. L.; He, H. Y.; Dai, F. N.; Sun, D. F.; Ke, Y. X. *Inorg. Chem.* **2010**, *49*, 8650. (c) Liu, C. M.; Zuo, J. L.; Zhang, D. Q.; Zhu, D. B. *CrystEngComm* **2008**, *10*, 1674. (d) Zhao, X. L.; He, H. Y.; Dai, F. N.; Sun, D. F.; Ke, Y. X. *Inorg. Chem.* **2010**, *49*, 8650. (e) Yang, L. F.; Cao, M. L.; Mo, H. J.; Hao, H. G.; Wu, J. J.; Zhang, J. P.; Ye, B. H. *CrystEngComm* **2009**, *11*, 1114. (f) Gándara, F.; de la Pena-o'Shea, V. A.; Illas, F.; Snejko, N.; Proserpio, D. M.; Gutierrez-Puebla, E.; Monge, M. A. *Inorg. Chem.* **2009**, *48*, 4707.
- (20) (a) Xue, M.; Zhu, G. S.; Li, Y. X.; Zhao, X. J.; Jin, Z.; Kang, E.; Qiu, S. L. *Cryst. Growth Des.* **2008**, *8*, 2478. (b) Chen, P. K.; Che, Y. X.; Xue, L.; Zheng, J. M. *Cryst. Growth Des.* **2006**, *6*, 2517. (c) Ockwig, N. W.; Delgado-Friedrichs, O.; O'Keeffe, M.; Yaghi, O. M. *Acc. Chem. Res.* **2005**, *38*, 176. (d) Liang, L. L.; Ren, S. B.; Zhang, J.; Li, Y. Z.; Du, H. B.; You, X. Z. *Cryst. Growth Des.* **2010**, *10*, 1307. (e) Baburin, I. A.; Blatov, V. A.; Carlucci, L.; Ciani, G.; Proserpio, D. M. *Cryst. Growth Des.* **2008**, *8*, 519. (f) Du, M.; Zhang, Z. H.; Tang, L. F.; Wang, X. G.; Zhao, X. J.; Batten, S. R. *Chem.—Eur. J.* **2007**, *13*, 2578.
- (21) (a) Liang, L. L.; Zhang, J.; Ren, S. B.; Ge, G. W.; Li, Y. Z.; Du, H. B.; You, X. Z. *CrystEngComm* **2010**, *12*, 2008. (b) Ma, D. Y.; Wang, W. X.; Li, Y. W.; Li, J.; Daiguebonne, C.; Calvez, G.; Guillou, O. *CrystEngComm* **2010**, *12*, 4372. (c) Zhang, J.; Bu, X. H. *Chem. Commun.* **2008**, 1756. (d) Du, M.; Zhao, X. J.; Guo, J. H.; Batten, S. R. *Chem. Commun.* **2005**, 4836. (e) Kostakis, G. E.; Malandrinos, G.; Nordlander, E.; Haukka, M.; Plakatouras, J. C. *Polyhedron* **2009**, *28*, 3227. (f) Su, C. Y.; Smith, M. D.; Goforth, A. M.; Zur Loyer, H. C. *Inorg. Chem.* **2004**, *43*, 6881.
- (22) Carlucci, L.; Ciani, G.; Proserpio, D. M.; Rizzato, S. *Dalton Trans.* **2000**, 3821.
- (23) (a) Yang, Q. Y.; Zheng, S. R.; Yang, R.; Pan, M.; Cao, R.; Su, C. Y. *CrystEngComm* **2009**, *11*, 680. (b) Chippindale, A. M.; Hibble, S. J. *J. Am. Chem. Soc.* **2009**, *131*, 12736. (c) Zhang, Z. H.; Chen, S. C.; Mi, J. L.; He, M. Y.; Chen, Q.; Du, M. *Chem. Commun.* **2010**, *46*, 8427. (d) Liu, T. F.; Lü, J.; Guo, Z. G.; Proserpio, D. M.; Cao, R. *Cryst. Growth Des.* **2010**, *10*, 1489.
- (24) (a) Uemura, K.; Maeda, A.; Maji, T. K.; Kanoo, P.; Kita, H. *Eur. J. Inorg. Chem.* **2009**, 2329. (b) Sculley, J. L.; Yuan, D. Q.; Zhou, H. C. *Energy Environ. Sci.* **2011**, *4*, 2721.
- (25) (a) Li, J. R.; Ma, Y. G.; McCarthy, M. C.; Sculley, J.; Yu, J. M.; Jeong, H. K.; Balbuena, P. B.; Zhou, H. C. *Coord. Chem. Rev.* **2010**, *255*, 1791. (b) Xiang, H.; Gao, W. Y.; Zhong, D. C.; Jiang, L.; Lu, T. B. *CrystEngComm* **2011**, *13*, 5825. (c) Chen, M. S.; Chen, M.; Takamizawa, S.; Okamura, T.; Fan, J.; Sun, W. Y. *Chem. Commun.* **2011**, *47*, 3787. (d) Zhong, D. C.; Lu, W. G.; Jiang, L.; Feng, X. L.; Lu, T. B. *Cryst. Growth Des.* **2010**, *10*, 739. (e) Zhang, Y. J.; Liu, T.; Kanegawa, S. J.; Sato, O. *J. Am. Chem. Soc.* **2010**, *132*, 912. (f) Liu, H. Y.; Yuan, Y. J.; Yu, Z. T.; Zou, Z. G. *CrystEngComm* **2011**, *13*, 2391. (g) Lama, P.; Ajiaz, A.; Neogi, S.; Barbour, L. J.; Bharadwaj, P. K. *Cryst. Growth Des.* **2010**, *10*, 3410.
- (26) (a) Yersin, H.; Vogler, A. *Photochemistry and Photophysics of Coordination Compounds*; Springer-Verlag: Berlin, 1987. (b) Xu, J. G.; Wang, Z. B. *Fluorescence Analytical Methods*; Chinese Science Publishing Company: Beijing, 2006.
- (27) (a) Guo, J.; Ma, J. F.; Liu, B.; Kan, W. Q.; Yang, J. *Cryst. Growth Des.* **2011**, *11*, 3609. (b) Yang, X. L.; Xie, M. H.; Zou, C.; Wu, C. D.

CrystEngComm **2010**, *12*, 1779. (c) Allendorf, M. D.; Bauer, C. A.; Bhakta, R. K.; Houk, R. J. T. *Chem. Soc. Rev.* **2009**, *38*, 1330. (d) Chang, Z.; Zhang, A. S.; Hu, T. L.; Bu, X. H. *Cryst. Growth Des.* **2009**, *9*, 4840.

(28) (a) Mu, Y. J.; Han, G.; Ji, S. Y.; Hou, H. W.; Fan, Y. T. *CrystEngComm* **2011**, *13*, 5943. (b) Zhou, X. X.; Fang, H. C.; Ge, Y. Y.; Zhou, Z. Y.; Gu, Z. G.; Gong, X.; Zhao, G.; Zhan, Q. G.; Zeng, R. H.; Cai, Y. P. *Cryst. Growth. Des.* **2010**, *10*, 4014. (c) Tekin, E.; Egbe, D. A. M.; Kranenburg, J. M.; Ullricht, C.; Rathgeber, S.; Birckner, E.; Rehmann, N.; Meerholz, K.; Schubert, U. S. *Chem. Mater.* **2008**, *20*, 2727. (d) Wang, S. N.; Xing, H.; Li, Y. Z.; Bai, J. F.; Pan, Y.; Scheer, M.; You, X. Z. *Eur. J. Inorg. Chem.* **2006**, 3041.